Athens Journal of Sciences - Volume 12, Issue 4, December 2025 – Pages 235-250

Study on the feasibility DLC coatings doped with Transition Metal Cu or Ag as Biosensing Electrode for Glucose

*By Jihua Peng**

Researching biosensing electrodes for glucose measurement is crucial for human health. These electrodes need to be accurate, reliable, and long-lasting. In this study, diamond-like carbon amorphous coatings were fabricated to contain nano-crystal Cu or Ag (a-C:Cu, a-C:Ag) by the complex deposition of the filtered cathode vacuum arc of graphite and magnetron sputtering of copper or silver. All electrodes showed good conductivity. The a-C:Cu electrodes had sp^3C fraction 29~45 %, while a-C:Ag had 26–42 at.%. The morphologies, microstructures, and the carbon hybridization structure, and the resistance of the specimens were characterized using SEM, XRD, Raman, XPS spectroscopy, and the four-point-probe. It is found that the catalytic activity of nano-crystal Cu particles (np-Cu) for glucose oxidation is not affected by a carbon layer on their surface, and this is different from nano-crystal Ag particles (np-Ag), which are sensitive to surface conditions. Thus, a-C:Cu, made by one-step vacuum deposition, is suitable for sensing glucose in an alkaline solution. The anodic peak current at 0.21 V vs. Hg/HgO increased in two log-linear regions with glucose content. However, in the 1M KCl+50 Mm $K_3Fe(CN)_6$, a-C:Cu and a-C:Ag cannot be used as glucose-sensing electrodes. The a-C:Ag coatings present challenges for glucose sensing due to difficulties in controlling the surface conditions of np-Ag.

Keywords: *Transition metal doping; Diamond-like carbon; Electrochemical performance; Glucose; Biosensing.*

Introduction

Diamond-like carbon (DLC) is a special form of amorphous carbon, which has a lot of sp^3 bonding and sp^2 bonding and offers excellent mechanical, physical, and chemical properties (Robertson 2000; Peng et al. 2021). These properties can be adjusted by doping and controlling layer structure during vapor deposition. DLCs are used on devices to enhance sealing, anti-corrosion, and anti-wear performance (Vetter 2014, Peng et al. 2022, Zhao et al. 2020). Adding transition metals like Cu or Ag to DLCs improves chemical bonding, adhesion, and overall performance (Markwitz et al. 2015, Yan C et al. 2023, Yan F et al. 2023). This makes coated devices operate well in ocean environments (Wei et al. 2020, Liu et al. 2016) and human body environment (Jastrzebski et al.2021, Birket et al. 2023, Towobola et al. 2025). In the energy sector, DLCs doped with Cu or Ag are strong candidates for metal bipolar plates and future supercapacitors (Tian et al. 2024, Buathong et al. 2025). In electrochemistry, DLCs are widely used as electrodes (Zeng et al. 2014). Transition metals Cu and Ag are key catalysts (Zhu et al. 2012, Jing et al. 2022, Dayakar et al. 2018). Combining the catalysis

*Associate Professor, School of Materials Science and Engineering, South China University of Technology, China.

https://doi.org/10.30958/ajs.12-4-1 doi=10.30958/ajs.12-4-1

of Cu or Ag with the broad electrochemical window of DLCs shows great promise for sensing biological and medical substances.

In recent years, there has been growing interest in creating sensors for blood glucose monitoring. These sensors aim to be selective, sensitive, responsive, and cost-effective for managing diabetes. Electrochemical biosensing has become the main approach. There are two main types: enzyme-based testing (Patolsky et al. 2004, Maalouf et al. 2007) and non-enzyme testing (Triroj et al.2020, Hwang et al. 2018). The latter has gained significant attention. For enzyme-free glucose-sensing electrodes, a catalytic substance is needed on the surface for glucose oxidation. Transition metals like copper, nickel, platinum, palladium, and silver have been suggested (Nagy et al. 2001, Naikoo et al. 2020, Usman et al. 2019). Some studies indicate that OH^- functional groups on the electrode can oxidize glucose without catalysts (Honda et al. 2013, Barragan et al. 2018). Currently, electrochemical deposition of catalytic species onto conductive substrates is the main method for creating enzyme-free electrodes (Wu et al. 2015, Dai et al. 2018, Aun et al. 2023). For DLC-based electrodes, a two-step fabrication process is used. First, DLCs are vapor deposited, then electrochemical deposition of the transition metal or compounds occurs. While these electrodes perform well in glucose sensing, they face issues like high costs and poor adhesion between the catalytic layer and substrate. Therefore, there is a need to explore a one-step fabrication method for DLC electrodes with transition metals and investigate their glucose biosensing potential.

The goal of this study is to create Cu or Ag doped DLC electrodes using a one-step method. We will examine their electrochemical performance in glucose electrolytes. For fabrication, we use a magnetically filtered cathode arc of graphite as the carbon source. We also use a direct current magnetron cathode of pure transition metal for the Cu or Ag source. This process embeds nano-crystal particles of Cu or Ag into the amorphous carbon matrix. We will explore the states of the doped Cu or Ag and their impact on bonding structure, surface morphology, and electrochemical performance. This study will help assess how well Cu/Ag doped DLC electrodes can measure glucose content in electrolytes.

After this introduction, we will present a section called "Literature Review." This will cover the catalysis of glucose oxidation by Cu and Ag, along with the status of transition metal-doped DLCs for glucose measurement. In the "Methodology" section, we will detail how to prepare DLC doped with Cu or Ag. We will also discuss the morphology, bonding structure, and electrochemical performance. The "Results and Discussion" section will showcase the main findings and provide insightful analysis. Finally, we will outline clear conclusion points.

Literature Review

Many studies show that in alkaline electrolytes, Cu or Cu-oxides can oxidize glucose (Nagy et al. 2001, Yang et al. 2010, Ma et al. 2019). The presence of Cu^{2+} in the solution also helps oxidize glucose (Zheng et al. 2019). When using the ferrocene derivative (FcCO-Glu-Cys-Gly-OH) to oxidize glucose, doped nanocrystal particles (np-) of Cu or Co act as electrocatalysts (Zhan et al. 2022). Similarly, np-Ag can promote glucose oxidation (Chen et al. 2012, Smikhovskaia et al.2019, Usman

et al. 2019). However, the oxidation of np-Ag in alkaline solutions depends on its fabrication method. When np-Ag is made with carbon secured from the extraction process (Dayakar et al. 2018) and through electrochemical deposition (Buathong et al. 2025), its oxidation is reduced. This indicates that np-Cu or Ag can enhance glucose oxidation in alkaline electrolytes. DLC-based electrodes with np-Cu or Ag are promising for measuring glucose concentration. Additionally, the state of np-Cu or Ag affects the surface morphology and electrochemical performance of the electrode.

Using one-step vapor deposition to create transition metal-doped DLC-based electrodes builds a composite structure. This structure includes np-transition metal and an amorphous carbon matrix. This method adjusts bonding and adhesion. As a result, it offers better conductivity and electrochemical performance than traditional glassy carbon electrodes (Maalouf et al. 2006, Kim et al. 2009). Additionally, low-temperature fabrication of DLC electrodes supports semiconductor integration. The electrochemical performance can be fine-tuned using appropriate dopants during vapor deposition (McCreery 2008). These dopants can include metal elements that enhance electro-catalysis for bio-compounds.

A layer of nanocrystal Au, Ag, or Cu can be deposited onto DLCs using post-electrochemical methods. This process helps catalyze glucose oxidation (Liu et al. 2010, Jin et al.2 012). However, there is less research on Cu/Ag-doped DLCs as glucose biosensors. It has been shown that Ni-doped DLC electrodes improve sensitivity to H_2O_2 in the electrolyte by controlling Ni content (Liu et al. 2018). TDLC electrodes doped with Cu or Cu-Ni demonstrate fast reaction rates for the inner-sphere redox couple $(Fe(CN)_6)^{3-/4-}$ (Wang et al. 2022). Ag-doped DLC electrodes show quasi-reversibility of the $Fe^{2+/3+}$ redox couple in KOH solution (Buathong et al. 2025). These DLCs with Cu or Ag dopants are expected to be good electrodes for glucose sensing. However, both their ability to measure glucose content and their electrochemical performance require further investigation.

Methodology

Sample Preparation and Post-treatment

Commercial single-crystal Si wafers (20.00 mm × 10.00 mm × 0.63 mm) and polished stainless-steel coupons were cleaned with ethanol and deionized water. This removed the surface contaminants. Then, they were dried under N_2 gas. The a-C coatings were deposited using a filtered cathode vapor arc (FCVA) system (Peng et al. 2024). In this system, a Ti target (99.99% purity), Ag target (99.99% purity), and Cu target (99.99% purity) were powered by direct current magnetron sputtering. The graphite cathode arc target (99.99% purity) used a pulsed direct current source. After placing the substrate samples in the vacuum chamber, the base pressure dropped below 2×10^{-3} Pa. An Ar gas flow (99.99% purity, 30 sccm) was supplied through the inlet. The chamber was heated to 150 °C during the entire deposition process.

First, a –1200 V direct current pulse bias voltage (V_b) was applied to the samples. They were etched for 30 minutes with Ar ions. Next, a Ti-interlayer of about 150–300 nm thickness was deposited using the Ti magnetron sputtering target at 3 kW. After turning off the Ti target, the graphite target was activated.

This prepared an a-C sub-layer for 45 minutes with a V_b of –1200 V. Finally, the a-C:Cu top layer was deposited for 90 minutes. Alternatively, a-C:Ag was deposited for 30–60 minutes, using a V_b of –650 V. This followed the Cu or Ag magnetron sputtering target conditions in Table 1. In total, four batches of a-C:Cu and six batches of a-C:Ag samples were prepared.

Table 1. *Process Parameters during Deposition and Metal Content in the Top Layer*

Batch No.	Cu target power /W	Ar flow /sccm	Cu-target shield	Cu content /at.%	Ag content /at.%
T1	100	28	Fully closed	1.1	-
T2	200	28	Fully closed	5.2	-
T3	400	25	Fully closed	13.5	-
T4	400	23	Half opened	23.6	-
Ag1#	10	28	Fully open	-	0.5
Ag2#	100	28	Fully closed	-	5.0
Ag3#	200	20	Fully closed	-	12.1
Ag4#	400	28	Fully closed	-	45.0
Ag5#	300	20	Fully closed	-	52.1
Ag6#	100	48	Fully open	-	79.9

Morphological and Chemical Bonding Structure Characterization

The coatings were analyzed using an X-ray diffraction (XRD) diffractometer (PANalytical, USA) with Cu Kα irradiation (40 kV, 40 mA, wavelength 0.15418 nm). We scanned 2θ from 30° to 60° and used a 2° grazing angle to reduce substrate signal intensity. We observed the composition, top surface images, and fractured cross-section of the coated Si wafers using field-emission scanning electron microscopy (FE-SEM) with EDS (SU5000, Japan; or Nova NANOSEM430, USA) at a 15 kV voltage. The hybridization states of the carbon atoms were determined with micro-Raman spectroscopy, using an Ar-ion laser with a 532 nm excitation wavelength and 5 mW power (LabRAM Arami, France). The scanning range was 100–4000 cm^{-1} for 300 seconds. We characterized chemical bond shifts using X-ray photoelectron spectroscopy (XPS; Axis Supra$^+$, Japan) at an incident photon energy of 1486.6 eV. The X-ray gun operated at a 5 mA emission current and 15 kV accelerating voltage. The XPS instrument was calibrated using the Au $4f^{7/2}$ core-level electron binding energy (84.00 eV) as a standard. Before each measurement, we etched the sample surface for 120 seconds with Ar ions at 2 keV and a 1 mA mm^{-2} current density to remove contaminants. We used the Shirley method for background subtraction, and analyzed the data with XPS Peak 4.1 software. For peak fitting, a Gaussian–

Lorentzian function with a Lorentzian fraction of 20% was applied, and the full-width at half maximum for C 1s, Cu 2p, and Ag 3d was fixed.

Conductivity and Electrochemical Performance Characterization

The resistivity of the coatings on the Si wafers was measured using a four-point sheet resistance probe (RTS9, Shenzheng Jundashidai Instrument Ltd., China). We analyzed the electrochemical properties of the DLC films using a three-electrode system on an electrochemical workstation (CompactStat.h, IVIUM, Netherlands) at room temperature. The cyclic voltammetry (CV) and differential pulse voltammetry (DPV) for this analysis was employed. During CV tests, we used scanning rates of 50, 100, 150, 200, 250, and 300 mVs^{-1}. The reference electrode was Ag/AgCl electrode when using a KCl-based electrolyte and an Hg/HgO electrode for NaOH-based electrolyte. A platinum foil (10 mm × 10 mm × 0.1 mm) served as the counter electrode. The working electrodes were a-C:Cu or A-C:Ag coated 316L substrates, each with an effective area of 1 cm^2. Compared to the normal hydrogen electrode (NHE), the zero-electrode potential of the Ag/AgCl is +0.244 V and that of the Hg/HgO electrode is +0.198 V.

All reagents in this work were analytical grade. They were dissolved in deionized water. This included potassium chloride, potassium ferricyanide, D-glucose, and nitric acid, all from Sigma-Aldrich®. Before use as working electrodes, the Cu or Ag-doped DLC films were cleaned. They were rinsed with acetone and double-distilled water for 10 minutes. To remove surface cotton-like particles that affect glucose sensing in an alkaline electrolyte, some a-C:Cu samples from a different batch were etched. This was done using a 1 M HNO_3 solution. The samples were immersed in the 1 M HNO_3 solution for 1 minute. After that, they were washed with tap water and then with deionized water. Finally, they were rubbed and dried with a cleanroom wiper. During the HNO_3 etching, a reaction likely occurred involving copper and Cu-oxides.

$$3Cu+8HNO_3\ (light) = 3Cu(NO_3)_2 + 2NO\uparrow + 4H_2O \quad (1)$$

$$CuO+2HNO_3 \rightarrow Cu(NO_3)_2 + H_2O \quad (2)$$

$$3Cu_2O+14HNO_3 = 6Cu(NO_3)_2 + 2NO\uparrow + 7H_2O \quad (3)$$

Results and Discussion

Coating Surface Morphology

The SEM images of as-deposited a-C:Cu coatings are in Figures 1a–1d, with cross-section images as insets. Figure 1e shows Cu-free a-C coatings, made when the magnetron sputtering Cu-target was off during the final step. The a-C coating has a total thickness of 1.53 μm and a smooth surface with small droplets under 500 nm. From previous EDS study, the small size droplets were carbon-enriched particles, which was emitted from the graphite arc target during evaporation. Three sublayers exist in the a-C:Cu coatings: the Ti-interlayer is about 320 nm thick, and the a-C sublayer, made at V_b of –1200 V, ranges from 300 to 309 nm thick. The top a-C:Cu layer thicknesses of samples T1–T4 are

about 629, 520, 978, and 1051 nm, respectively. The XRD pattern of these a-C:Cu samples are in Figure 1f, with their Cu contents in Table 1. Increasing Cu content in the DLCs led to more nanocrystalline Cu grains in the coatings (Liu et al.2016). The SEM images of as-deposited a-C:Ag coatings are in Figures 2a–2e, also with cross-section insets. Unlike the a-C:Cu samples, the a-C:Ag coatings have a smooth surface with fewer droplets. As Ag content increases, the fraction of Ag-crystal grains also rises, as shown in Figure 2f.

Droplets are unavoidable when using the graphite arc to deposit DLCs (Peng et al. 2023), like the a-C coating in Figure 1e. In this study, cotton-like particles on the surface may affect the shield's sealing in front of the metal-target. These particles ignite after the a-C sub-layer deposition at –1200 V. Carbon ash sticks to the metal-target surface and gets sputtered out when the target ignites. This carbon ash forms more easily on the Cu-target than on the Ag-target.

Coating Composition, and the Bonding Microstructure

The Raman spectra provide key insights into carbon atom hybridization, hydrogen content, and residual stress in DLCs (Robertson 2000, Vetter 2014). Figures 3a and 4a show the spectra for as-deposited a-C:Cu and a-C:Ag coatings, respectively. These spectra were fitted using the double Gaussian method. The G peak at about 1555 cm^{-1} reflects the in-plane breathing vibration of sp^2C sites. In contrast, the D peak at 1370 cm^{-1} indicates the out-plane bending vibration of aromatic ring-like sp^2C and disordering (Liu et al. 2016, Peng et al. 2021). Typically, the intensity ratio of the D peak to the G peak (I_D/I_G) is inversely related to the sp^3C fraction in DLCs. It is also positively correlated to the size of ring-like sp^2C clusters when they are under 2 nm. Many factors affect the G peak position (G_{peak}), including the sp^2C fraction and residual stress in the coating. More disordering in the coating leads to a larger full width at half maximum of the G peak ($FWHM_G$). Table 2 shows the fitted parameters for the a-C:Cu and a-C:Ag coatings, along with their resistivity and the ratio of $sp^2C{=}C/sp^3C{-}C$ bonds from XPS fitting. According to previous studies (Zhou 2016, Jing et al. 2022, Yan Cet al. 2023), increasing the Cu or Ag content in the coating enhances the sp^2C fraction, ordering extent, and sp^2C cluster size, while reducing residual stress.

Figure 1. *SEM Images (a–e) of the Top Surface and Cross-section of the Coatings with different Cu Content, as well as their XRD Pattern (f)*

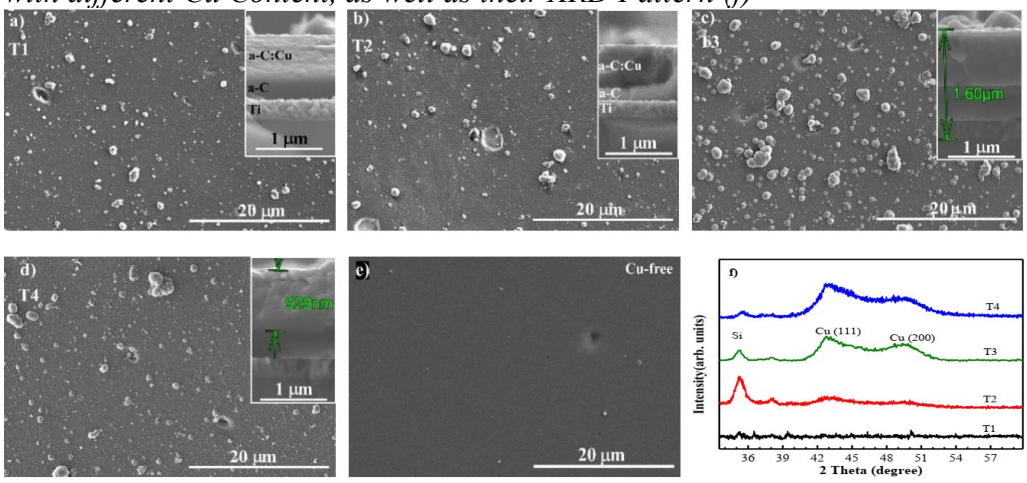

Figure 2. *SEM Images (a–e) of the Top Surface and Cross-section of the Coatings with different Ag Content, as well as their XRD Pattern (f)*

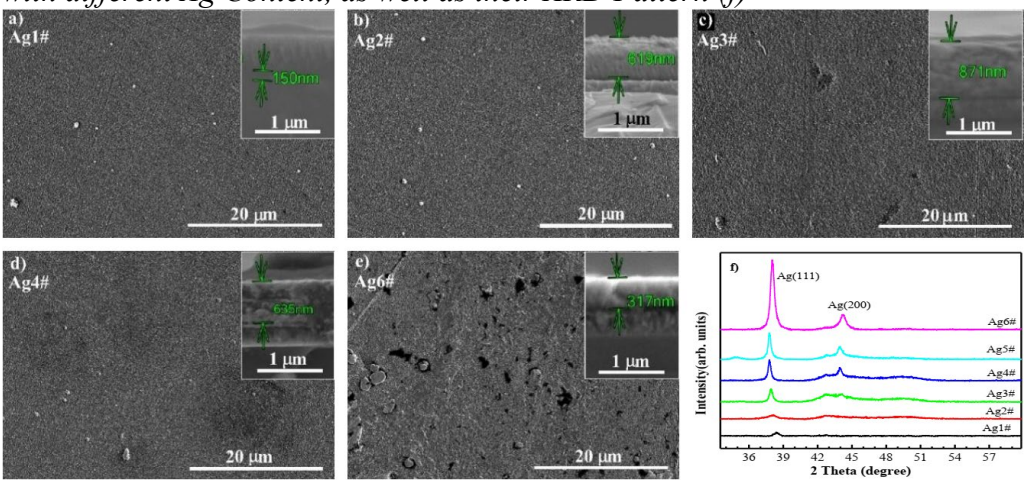

XPS is useful for characterizing the hybrid structure of carbon atoms at the surface. Its resolution is less than 5 nm. The C 1s and Cu 2p XPS spectra of the Cu-doped coatings are shown in Figures. 3b and 3c. Previous studies (Robertson 2000, Jin et al. 2012, Peng et al. 2024) report four peaks in the XPS spectra. These peaks correspond to different core orbital binding energies: sp^2C=C (284.4 ± 0.2 eV), sp^3C–C (285.1 ± 0.2 eV), C–O (286.4 ± 0.2 eV), and C=O (288.2 ± 0.2 eV). Cu atoms in the DLCs mostly exist in metallic states. They bond poorly with carbon (Khan et al. 2019, Wang et al. 2022). Some Cu–O bonds likely form as CuO or Cu_2O due to reactions with the atmosphere (Aun et al. 2023). The sp^2C=C/sp^3C–C ratio from XPS fitting matches the Raman analysis results. It is hard to differentiate the Cu $2p^{3/2}$ and Cu $2p^{1/2}$ peaks from metallic Cu or Cu-oxides. Thus, we assume Cu mainly exists in the metallic state, which aligns with the XRD pattern in Figure 1f. The C 1s and Ag 3d XPS spectra of the Ag-doped coatings are shown in Figures. 4b and 4c. Like the a-C:Cu coatings, carbon atoms in a-C:Ag coatings mainly take the form of sp^2C and sp3C sites. The Ag $3d^{3/2}$ (374.4 eV) and Ag $3d^{5/2}$ (368.4 eV) peaks were seen in the Ag-doped DLC (Liu et al. 2018, Yan et al. 2023). This indicates Ag atoms in the coatings form metallic Ag-clusters or Ag-crystals.

The conventional glassy carbon electrode shows that Cu solid-solution in sp^2C clusters likely caused more disorder. At higher Cu content, the cotton-like particles grew in size and density, which hindered electron transport. This led to an increase in resistivity (ρ) as Cu content rose. This finding contrasts with results in Ref (Khan et al. 2019). The doping of metallic Ag particles gives a-C:Ag better conductivity (Yan et al .2023).

Figure 3. *Raman Spectra (a) and XPS Spectra of C 1s (b) and Cu 2p (c) from different a-C:Cu Coatings*

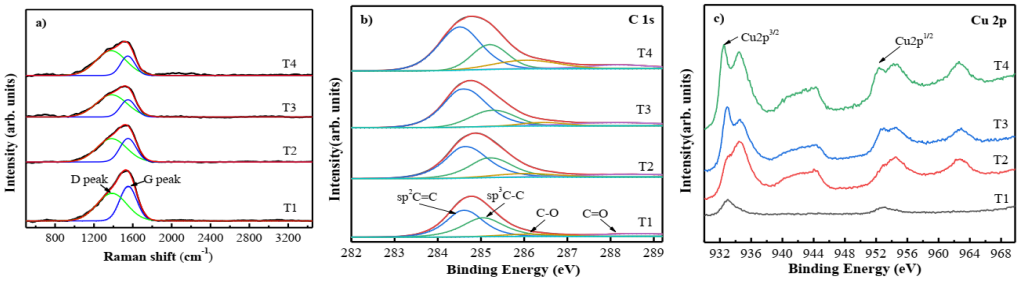

Figure 4. *Raman Spectra (a) and XPS Spectra of C 1s (b) and Ag 3d (c) from different a-C:Ag Coatings*

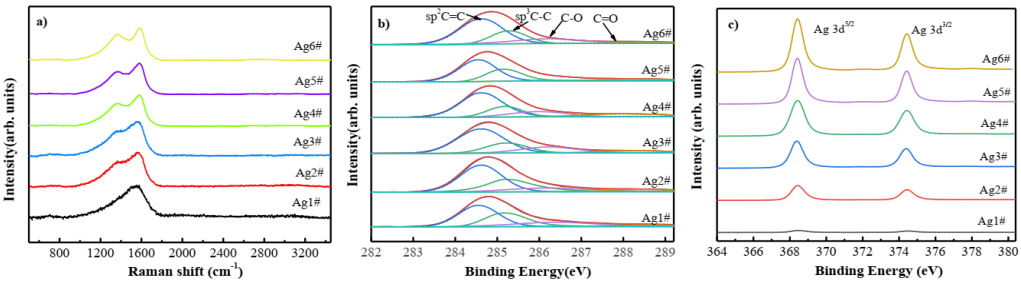

Table 2. *Resistivity and Peak Fitting Results from Raman/XPS Spectra of DLCs Coatings*

Specimen	I_D/I_G	G_{peak}/cm^{-1}	$FWHM_G$ cm^{-1}	sp^2/sp^3	ρ/Ω·m
T1	0.80	1552	205.2	1.19	4.76E-6
T2	0.99	1551	198.7	1.28	5.43E-6
T3	1.29	1550	182.4	2.50	6.26E-6
T4	1.28	1548	173.9	2.08	6.79E-6
Ag1#	0.72	1560	208.5	1.37	4.74E-8
Ag2#	1.09	1570	139.4	1.61	4.56E-8
Ag3#	1.15	1569	140.1	2.77	1.27E-7
Ag4#	1.03	1582	114.4	2.60	6.41E-8
Ag5#	1.19	1586	107.2	1.90	4.92E-8
Ag6#	1.06	1589	106.5	2.47	1.25E-8

Electrochemical Performance of DLCs Electrode in 1 M KCl with 50 mM $K_3Fe(CN)_6$ Electrolyte

<u>* T2 Electrodes</u>

The T2 coating had many nanocrystalline Cu and good conductivity. Thus, it was chosen as a suitable electrode for electrochemical experiments. Using Ag/AgCl as the reference electrode, setting scanning rates as 50, 100, 250, 200, 250, and 300 mV s^{-1}, Figure 5a presents the CV curves in 1 M KCl + 50 mM $K_3Fe(CN)_6$ electrolyte at different scanning rates. A pair of peaks appeared, indicating the redox

of the $(Fe(CN)_6)^{3-/4-}$ couple. As the scanning rate climbed from 50 to 300 mV s^{-1}, the potential difference between the anodic and cathodic peaks (ΔE_p) grew from 142 to 420 mV. The peak current ratio (I_a/I_c) reached 1.09, 2.01, 2.07, 2.22, 2.50, and 2.41, respectively. The quasi-reversibility of the $(Fe(CN)_6)^{3-/4-}$ couple was maintained at a slow scanning rate of 50 mV s^{-1} but worsened at higher rates. An anodic peak appeared at 0.71 V at 50 mV s^{-1}. This could be due to either the passivation of the carbon film (Turyan 2015) or the transformation of $Cu^{2+/3+}$ (Nagy et al. 2001, Aun et al. 2023). Compared to electrodes like B/N doped ta-C (Weber et al. 2024) and (Nb:N)-DLC (Liu et al. 2017), the T2 electrode in this study showed poorer quasi-reversibility for the $(Fe(CN)_6)^{3-/4-}$ couple. This is likely due to cotton-like particles on the T2 electrode. These particles may have affected the density of electron states, electron transfer, and the availability of active sites for reagent absorption (McCreery 2008, Markwitz et al. 2017).

Adding glucose concentration of 450 to 1170 mg L^{-1} into the electrolyte of 1M KCl+50 Mm $K_3Fe(CN)_6$, and setting the scanning rate at 50 mV s^{-1}, we analyzed the CV curves from the T2 electrode in Figure 5b. These curves show that the redox current pairs with glucose differ significantly from those without it. In the presence of glucose, the anodic peak potential varied widely, from 0.461 to 1.344 V. The anodic current peak ranged from 3.864 to 11.562 mA cm^{-2}. This suggests that multiple surface reactions control the anodic and cathodic peaks, not just the redox of the $(Fe(CN)_6)^{-3/-4}$ couple. Potential reactions include: 1) oxidation of OH^- radicals on the electrode surface (Honda et al. 2013); and 2) glucose oxidation catalyzed by $Cu^{2+/3+}$ reactions, along with the transformation of Cu itself (Yang et al. 2010, Zheng et al. 2019). Thus, the a-C:Cu electrode is unsuitable as a glucose biosensor in the KCl–$K_3Fe(CN)_6$ electrolyte system. Excessive reactions on the electrode surface complicate the differentiation of effects.

<u>* Ag2# Electrodes</u>

We selected Ag2# as the electrodes to study their electrochemical behavior based on conductivity and np-Ag content. Figure 6a shows the CV curves from the Ag2# electrode in a 1 M KCl + 50 mM $K_3Fe(CN)_6$ electrolyte at different scanning rates. An obvious redox peak from the $(Fe(CN)_6)^{3-/4-}$ couple appeared. However, the redox reaction was not fully reversible, even at a slow scanning rate of 50 mV.s^{-1}. At scanning rates of 50, 200, and 300 m mV.s^{-1}, the anodic peak current increased from 3.90 mA.cm^{-2} to 7.02 mA.cm^{-2}. This suggests that the surface electrochemical reaction is limited by diffusion (Dayakar et al. 2018, Smikhovskaia et al. 2019). For these rates, the I_a/I_c ratios were 0.90, 0.96, and 0.98, while the ΔE_p values were 500, 770, and 860 mV, respectively. In comparison, the electrochemically deposited np-Ag electrode (Zhao et al. 2021) showed better reversibility for the $(Fe(CN)_6)^{3-/4-}$ couple. The lower reversibility in Ag2# may result from the np-Ag being wrapped by the amorphous carbon matrix.

Adding glucose concentration from 270 to 1170 mg L^{-1} to the electrolyte of 1M KCl+50 mM $K_3Fe(CN)_6$, and setting the scanning rate at 50 mV. s^{-1}, the CV curves from the Ag2# electrode are shown in Figure 6b. The curves with and without glucose are similar. The anodic and cathodic peak currents mainly show the redox reaction of the $(Fe(CN)_6)^{3-/4-}$ couple. However, the anodic peak current changes non-linearly with the glucose concentration. The density and size of np-Ag influence the electron transfer resistance (R_{ct}) of $(Fe(CN)_6)^{3-/4-}$ reaction on the graphene@Ag electrodes (Zhao 2021). Additionally, glucose adsorbs onto active silver sites, reducing the current. Meanwhile, Ag ions dissolve into the solution, promoting glucose oxidation

and increasing anodic current. Although these effects on the current are small, they create a nonlinear relationship with glucose content. Thus, the a-C:Ag electrode is also unsuitable as a glucose biosensor in the in the KCl–$K_3Fe(CN)_6$ electrolyte system.

Figure 5. *CV Curves of T2 Electrode in the 1 M KCl + 50 mM $K_3Fe(CN)_6$ Electrolyte: a) with and b) without Glucose*

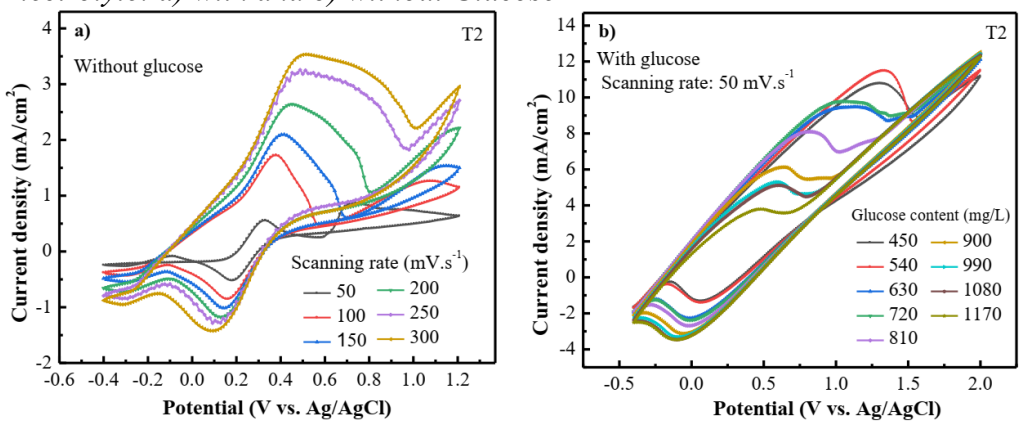

Figure 6. *CV Curves of Ag2# Electrode in the 1 M KCl + 50 mM $K_3Fe(CN)_6$ Electrolyte: a) with and b) without Glucose*

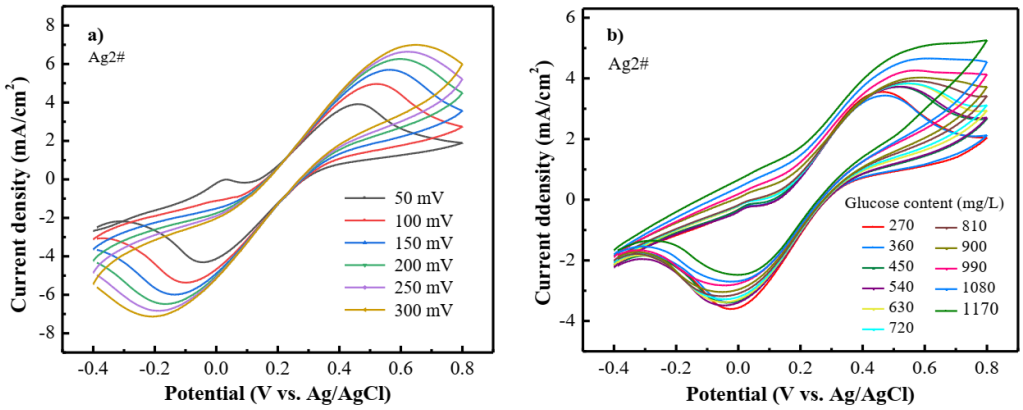

Electrochemical Performance of DLCs Electrode in 1 M NaOH Electrolyte

<u>* T2 Electrodes</u>

The oxidation reactions $Cu^{0/+}$, $Cu^{+/2+}$, and $Cu^{2+/3+}$ occur in alkaline electrolyte. Notably, $Cu^{2+/3+}$ boosts glucose oxidation (Nagy et al. 2001, Barragan et al. 2018, Zheng et al. 2019). With a scanning rate of 50 mV s^{-1} and a Hg/HgO reference electrode, Figure 7a shows the CV curves of the a-C:Cu electrodes in 1 M NaOH. The oxidation potentials for $Cu^{0/+}$, $Cu^{+/2+}$, and $Cu^{2+/3+}$ were marked. At about 900 mV, the anodic currents for T1–T4 electrodes were 73, 58, 70, and 97 μA cm^{-2}, respectively. These values are much higher than that of the pure Cu electrode (Nagy et al. 2001). This suggests that a-C:Cu electrodes have high reactivity due to the coatings, which include nanocrystalline Cu, metallic Cu clusters, and Cu–O bonds, either within the coating matrix or in the cotton-like particles. Thus, a-C:Cu-coated electrodes are promising for glucose biosensing in alkaline electrolytes.

Many studies have explored glucose's electrocatalytic oxidation using copper and Cu-oxide electrodes in alkaline electrolyte. The potential for glucose oxidation by $Cu^{2+/3+}$ is around 0.3–0.65 V vs. Ag/AgCl (Dai et al. 2018, Ma et al. 2019, Zhan et al. 2022). Some reports indicate it is below 0 V vs. Ag/AgCl (Wu et al. 2015, Barragan et al. 2018). This varies based on electrode surface, solution pH, and Cu's form. The oxygen evolution reaction occurs at 0.23 V vs. Hg/HgO on the pure copper electrode in pH 14 electrolyte, according to the Pourbaix E–pH diagram for copper. In a 1 M NaOH + 0.1 M glucose electrolyte, Figure 7b shows the CV curves of T1–T4 electrodes at a 50 mV s^{-1} scanning rate. T1–T3 show an anodic current peak around 0.21 V vs. Hg/HgO, with current densities from 92 to 217 μA cm^{-2}. This suggests $Cu^{2+/3+}$ catalyzes glucose oxidation. As Cu content in the coatings increases, the oxidation current also rises. Examining the surface morphology in Figure 1, the catalytic activity of the Cu particles appears unaffected by the carbon layer covering. However, glucose readily adheres to the cotton-like particles, which weakly attach to the surface. This forms a dense glucose film barrier on T4 electrodes with high particle density. It protects the electrode surface from the electrolyte, leading to nearly zero reaction current. This is due to gluconolactone, the reaction product, being hard to desorb (Zheng et al. 2019) and diffuse into the solution. Overall, the current peaks above 0.21 V vs. Hg/HgO for T1–T3 electrodes result from glucose oxidation aided by copper ions in the electrolyte and absorbed OH^- groups. Therefore, the anodic current above 0.2 V vs. Hg/HgO directly relates to the glucose content.

Figure 7. *CV Curves of the a-C:Cu Electrodes in 1 M NaOH Electrolyte without (a) and with Glucose*

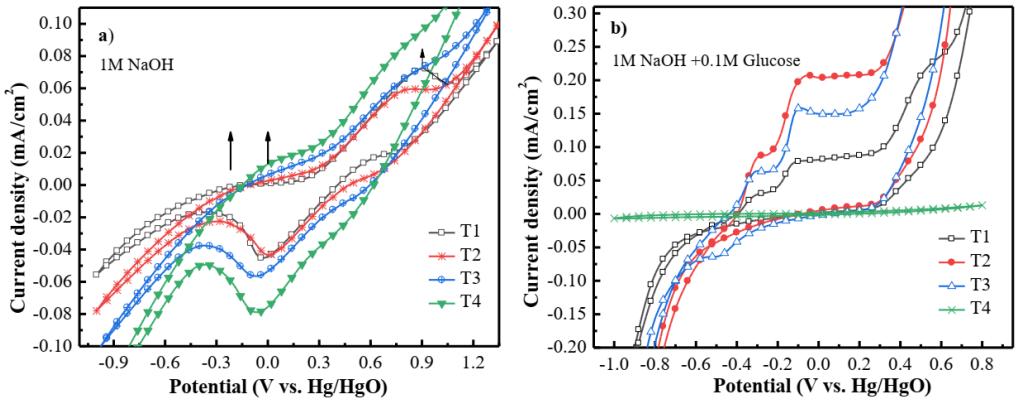

<u>* Ag2# Electrodes</u>

In this subsection, the scanning rate was set at 50 mV s–1. The voltage range was from –1.0 to 1.0 V, using Hg/HgO as the reference electrode. Figure 8a shows the CV curves of a-C:Ag electrodes with varying Ag content in 1 M NaOH. The current density remained below 10 μA.cm^{-2}, indicating that Ag, whether as Ag-cluster or np-Ag, is difficult to oxidize. Recent studies noted that np-Ag electrodes oxidize at specific voltages: Ag→AgOH at 0.34 V and Ag→Ag_2O at 0.73 V vs. Ag/AgCl (Usman et al. 2019). However, many reports state that np-Ag can catalyze glucose oxidation in alkaline solutions at potentials between 0.4–0.6 V vs. Ag/AgCl (Dayakar et al. 2018, Smikhovskaia et al. 2019), provided that the np-Ag has direct contact with the electrolyte. In this study,

silver and carbon were co-deposited. The np-Ag was either wrapped in an amorphous carbon matrix or covered by a carbon layer on the surface. This reduced the amount of np-Ag that directly contacted the solution, hindering its oxidation during potential scanning. After adding 0.1 M glucose to the 1 M NaOH electrolyte, the CV curves for all a-C:Ag electrodes are shown in Figure 8b. At 0.4 V vs. Hg/HgO, the Ag5# electrode displayed an anodic current of about 200 $\mu A.cm^{-2}$, indicating glucose oxidation by the silver catalyst. In contrast, other a-C:Ag electrodes showed only slight catalytic activity for glucose oxidation. This suggests that the catalytic activity of np-Ag depends on the area that directly contacts the solution. A similar observation was made with coated electrodes where Ag and carbon were deposited together (Dayakar et al. 2018, Buathong et al. 2025). Due to this sensitivity in catalytic activity, a-C:Ag electrodes face significant challenges as sensors for measuring glucose in alkaline electrolytes.

Feasibility of the a-C:Cu Electrode as a Glucose Sensor in an Alkaline Electrolyte

The weak adhesion of cotton-like particles on the surface can affect measurement reproducibility. To address this, we selected the T2 electrode for this section. We modified its surface using nitric acid etching (Formula (1–3)) to remove the particles, leaving craters behind. We recorded the CV curves in Figure 9a using a scanning rate of 50 mV s^{-1}, within a range of –1.0 to 1.0 V, in 1 M NaOH-based electrolytes with varying glucose concentrations. The anodic current peak appeared at 0.2–0.4 V vs. Hg/HgO, mainly due to glucose oxidation. To improve measurement precision, we employed the DPV method (Zhan et al. 2022) at a scanning rate of 4 mV s^{-1}, in the range of –0.2 to 0.6 V. The DPV curves are shown in Figure 9b. As glucose concentration increased, the peak current at 0.25 V vs. Hg/HgO rose steadily. Figure 9c illustrates the relationship between peak current and glucose content. We observed two linear regions with different slopes: one from 270 to 720 mg L^{-1} glucose, and another from 720 to 1080 mg L^{-1} glucose.

This finding slightly differs from reports by Yang et al. (2010) and Ma et al. (2029), which noted only one linear region in the measurement range. This difference stems from the surface condition of the etched T2 electrode, which had craters. The size of the glucose molecule is too large to enter the small craters. Thus, it gets absorbed by the active sites on the flat surface when glucose concentration is low. At high glucose concentrations, the active sites on the flat area become fully covered. Some glucose then "squeezes" into the craters, where copper ion concentration is high. Therefore, ensuring a smooth and uniform a-C:Cu electrode surface is crucial for the ongoing study.

Figure 8. *CV Curves of the a-C:Ag Electrodes in 1 M NaOH Electrolyte without (a) and with Glucose*

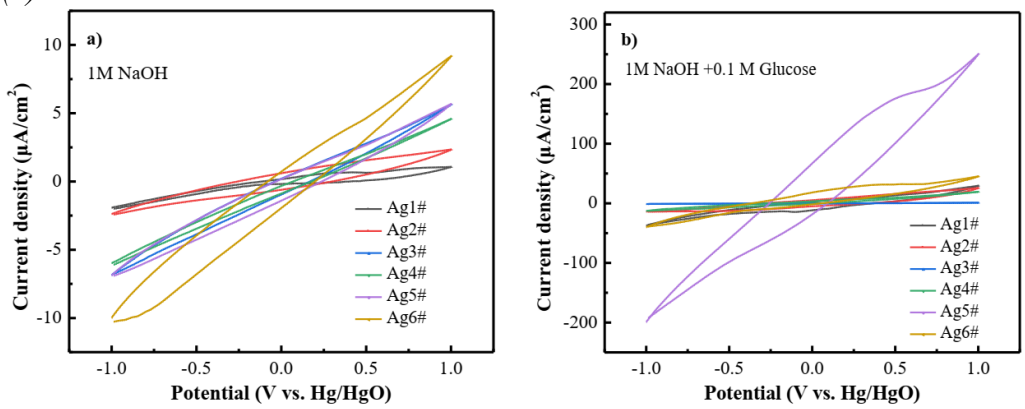

Figure 9. *CV Curves (a), DPV curves (b) from the etched T2 Electrode in 1 M NaOH Electrolyte with different Glucose Content, together with the Dependence between Glucose and Peak Anodic Current (c)*

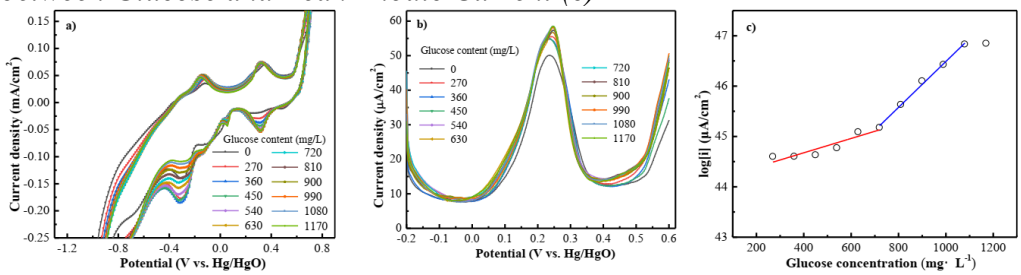

Conclusion

1) This study shows that a-C:Cu or a-C:Ag electrodes with nano-crystal particles (np-) can be made in one step. This uses a complex method that combines filtered cathode arc and magnetron sputtering deposition. The nps-Cu or Ag particles are wrapped in a carbon matrix. Those on the surface have a layer of carbon. As the Cu/Ag content increases, the sp^2C fraction and np-metal content also increase. During the a-C:Cu deposition, many cotton-like particles appeared on the surface. This was linked to the shield condition in front of the Cu target.

2) In the 1M KCl + 50 mM $K_3Fe(CN)_6$ electrolyte, the as-deposited T2 electrode with 5.2 at.% Cu showed a quasi-reversible behavior for the $(Fe(CN)_6)^{-3/-4}$ redox couple at a slow scanning rate. However, it degraded at higher rates. When 450 – 1170 mg/L glucose was added, reactions on the electrode surface included the $(Fe(CN)_6)^{-3/-4}$ redox, oxidation of OH^- groups and Cu, and oxidation driven by $Cu^{2+/3+}$. Therefore, the a-C:Cu electrode was not suitable as a glucose biosensor in this electrolyte system.

3) In the same electrolyte, the as-deposited Ag5# electrode with 5.0 at.% Ag showed poor reversibility for the $(Fe(CN)_6)^{-3/-4}$ redox couple at scanning rates from 50 to 300 $mV.s^{-1}$. After adding 450 – 1170 mg/L glucose, the anodic peak current was mainly due to the $(Fe(CN)_6)^{-4/-3}$ oxidation. Only a small amount of current came from silver-catalyzed glucose oxidation, which did not correlate linearly with glucose content. In a 1 M NaOH electrolyte, the metallic Ag

particles in the a-C:Ag electrodes remained unoxidized. The catalytic oxidation of glucose by np-Ag was highly affected by its surface condition, which was difficult to control. Thus, the a-C:Ag electrode was also unsuitable as a glucose biosensor in both electrolyte systems.

4) In alkaline electrolyte, the catalytic oxidation activity of np-Cu for glucose was not sensitive to its surface condition, whether covered by a carbon layer or not. However, the carbon layer significantly reduced the catalytic activity of np-Ag. The $Cu^{2+/3+}$ reaction promoted glucose oxidation at a potential of 0.2 – 0.3 V vs. Hg/HgO. The relationship between anodic peak current and glucose content showed two log-linear regions. This likely relates to the surface condition of the studied T2 electrode.

Acknowledgment

This study was financially supported by Guangzhou Grandtech Co., Ltd. (grant numbers 2023440002002575 and 2024440002002824).

Reference

Barragan J, Kogikoski S Jr, da Silva ET, Kubota L (2018) Insight into the electro-oxidation mechanism of glucose and other carbohydrates by CuO-based electrodes. *Analytical Chemistry* 90: 3357–3365.

Birkett M, Zia A, Devarajan D, Soni M, Panayiotidis M, Joyce T, *et al.* (2023) Multi-functional bioactive silver- and copper-doped diamond-like carbon coatings for medical implants. *Acta Biomaterialia* 167: 54–68.

Buathong S, Harnchana V, Pimsawat A, Jarernboon W, Pimanpang S, Amornkitbamrung V (2025) Electrodeposition of Ag-doped diamond-like carbon films on stainless steel for supercapacitor applications. *Journal of Alloys and Compounds* 1010: 177942.

Dayakar T, Rao K, Parb J, Sadasivuni K, Rao K, Rambabu N (2018) Non-enzymatic biosensing of glucose based on silver nanoparticles synthesized from *Ocimum tenuiflorum* leaf extract and silver nitrate. *Materials Chemistry and Physics* 216: 502–507.

Dai Y, Molazemhosseini A, Abbasi K, Liu C (2018) A cuprous oxide thin film non-enzymatic glucose sensor using differential pulse voltammetry and other voltammetry methods and a comparison to different thin film electrodes on the detection of glucose in an alkaline solution. *Biosensors* 8: 4.

Hwang D, Lee S, Seo M, Chung T (2018) Recent advances in electrochemical non-enzymatic glucose sensors—A review. *Analytica Chimica Acta* 1033: 1–34.

Jastrzebski K, Białecki J, Jastrebska A, Kaczmarek A, Para M, Niedzielski P, *et al.* (2021) Induced biological response in contact with Ag- and Cu-doped carbon coatings for potential orthopedic applications. *Materials* 14: 1861.

Jin C, Zeng A, Cho S, Boo J (2012) Investigation of copper and silver nanoparticles deposited on a nitrogen-doped diamond-like carbon (N-DLC) film electrode for biosensing. *Journal of the Korean Physical Society* 60: 912–915.

Khan M, Adil F, Majeed S, Farooq W, Hasan M, Jabeen R, *et al.* (2019) Structural, morphological, electrical and optical properties of Cu-doped DLC thin films. *Materials Research Express* 6: 126420.

Liu Y, Guo P, He X, Li L, Wang A, Li H (2016) Developing transparent copper-doped

diamond-like carbon films for marine antifouling applications. *Diamond and Related Materials* 69: 144–151.

Liu C, Chen W, Sun Y, Lin C (2018) Fabrication and electrochemistry characteristics of nickel-doped diamond-like carbon film toward applications in non-enzymatic glucose detection. *Applied Surface Science* 436: 967–973.

Liu N, Zhu H, Wei Q, Long H, Deng Z, Yu Z, *et al.* (2017) A niobium and nitrogen co-doped DLC film electrode and its electrochemical properties. *Journal of the Electrochemical Society* 164: H1091–H1098.

Maalouf R, Chebib H, Saikali Y, Vittori O, Sigaud M, Garrelie F, *et al.* (2007) Characterization of different diamond-like carbon electrodes for biosensor design. *Talanta* 72: 310–314.

Markwitz A, Leveneur J, Gupta P, Suschke K, Futter J, Rondeau M (2015) Transition metal ion implantation into diamond-like carbon coatings: Development of a base material for gas sensing applications. *Journal of Nanomaterials* 2015: 706417.

Naikoo G, Salim H, Hassan I, Awan T, Arshad F, Pedram M, *et al.* (2021) Recent advances in non-enzymatic glucose sensors based on metal and metal oxide nanostructures for diabetes management—A review. *Frontiers in Chemistry* 9: 748957.

Nagy L, Nagy G, Hajos P (2001) Copper electrode-based amperometric detector cell for sugar and organic acid measurements. *Sensors and Actuators B* 76: 494–499.

Patolsky F, Weizmann Y, Willner I (2004) Long-range electrical contacting of redox enzymes by SWCNT connectors. *Angewandte Chemie International Edition* 43: 2113–2117.

Peng J, Liao J, Zhang G, Huang J, Qiu X (2023) Microstructure evolution and mechanical performance of tetrahedral amorphous carbon coatings with dense droplets during annealing. *Materials Chemistry and Physics* 301: 127697.

Peng J, Li X, Li B, Liao J (2024) Controlling adhesion and thermal stability of tetrahedral amorphous carbon coatings with intermediate sp^3C fraction. *Thin Solid Films* 788: 140151.

Peng J, Xiao Y, Yang M, Liao J (2021) Effect of nitrogen doping on the microstructure and thermal stability of diamond-like carbon coatings silicon and oxygen. *Surface and Coatings Technology* 432: 127479–127488.

Peng Y, Peng J, Wang Z, Xiao Y, Qiu X (2022) Diamond-like carbon coatings in the biomedical field: Properties, applications and future development. *Coatings* 12: 1088.

Robertson J (2002) Diamond-like amorphous carbon. *Materials Science and Engineering R* 37: 129–281.

Tian F, Tao X, Wang J, Huang Z, Tian W, Chen J (2024) Investigation of Cu-doped amorphous carbon film in improving corrosion resistance and interfacial conductivity of proton exchange membrane fuel cell. *Surface and Coatings Technology* 485: 130926.

Towobola A, Jack T, Hosseini V, Yang Q (2025) Synthesis and characterization of Ag-doped DLC films for biomedical implants. *Diamond and Related Materials* 152: 111884.

Vetter J (2014) 60 years of DLC coatings: Historical highlights and technical review of cathodic arc processes to synthesize various DLC types, and their evolution for industrial applications. *Surface and Coatings Technology* 257: 213–240.

Wei J, Guo P, Liu L, Li H, Li H, Wang S, *et al.* (2020) Corrosion resistance of amorphous carbon film in 3.5 wt% NaCl solution for marine application. *Electrochimica Acta* 346: 136282.

Wu W, Periasamy A, Lin G, Shih Z, Chang H (2015) Palladium copper nanosponges for electrocatalytic reduction of oxygen and glucose detection. *Journal of Materials Chemistry A* 3: 9675–9681.

Yan C, Guo P, Zhou J, Chen R, Wang A (2023) Dependence of piezoresistive behavior upon Cu content in Cu-DLC nanocomposite films. *Diamond and Related Materials* 136: 109935.

Yan F, Jiang B, Liu B, Yang C, Dong D, Shi J (2023) Retention mechanism and conductivity

corrosion resistance performance of Ag-doped GLC and TiN films for metal bipolar plates. *Vacuum* 208: 111702.

Zeng A, Neto V, Gracio J, Fan Q (2014) Diamond-like carbon (DLC) films as electrochemical electrodes. *Diamond and Related Materials* 43: 12–22.

Zhan T, Feng X, An Q, Li S, Xue M, Chen Z, *et al.* (2022) Enzyme-free glucose sensors with efficient synergistic electrocatalysis based on a ferrocene derivative and two metal nanoparticles. *RSC Advances* 12: 5072–5079.

Zhao Z, Yu X, Zhang Z, Shu W, Li J (2020) Attempting Ag-doped diamond-like carbon film to improve seal performance of hydraulic servo-actuator. *Materials* 13: 2618.

Zhou B, Liu Z, Piliptsou D, Yu S, Wang Z, Rogachev A, *et al.* (2016) Structure and optical properties of Cu-DLC composite films deposited by cathode arc with double-excitation source. *Diamond and Related Materials* 69: 191–197.

Zhu Z, Garcia-Gancedo L, Flewitt A, Xie H, Moussy F, Milne W (2012) A critical review of glucose biosensors based on carbon nanomaterials: carbon nanotubes and graphene. *Sensors* 12: 5996–6022.